Energy Conversion and Management 243 (2021) 114423

Contents lists available at ScienceDirect

Energy Conversion and Management

journal homepage: www.elsevier.com/locate/enconman

Preliminary design of a fuel cell/battery hybrid powertrain for a heavy-duty yard truck for port logistics

G. Di Ilio [a,b,*], P. Di Giorgio [a,b], L. Tribioli [c], G. Bella [c], E. Jannelli [a,b]

[a] University of Naples 'Parthenope', Centro Direzionale, Isola C4, Naples 80143, Italy
[b] ATENA Future Technology, Centro Direzionale, Isola C4, Naples 80143, Italy
[c] University of Rome 'Niccolo Cusano', Via Don Carlo Gnocchi 3, Rome 00166, Italy

ARTICLE INFO

Keywords:
Energy conversion
Sustainable mobility
Fuel cells
Hydrogen technologies
Hybrid powertrains

ABSTRACT

The maritime transport and the port-logistic industry are key drivers of economic growth, although, they represent major contributors to climate change. In particular, maritime port facilities are typically located near cities or residential areas, thus having a significant direct environmental impact, in terms of air and water quality, as well as noise. The majority of the pollutant emissions in ports comes from cargo ships, and from all the related ports activities carried out by road vehicles. Therefore, a progressive reduction of the use of fossil fuels as a primary energy source for these vehicles and the promotion of cleaner powertrain alternatives is in order.

The present study deals with the design of a new propulsion system for a heavy-duty vehicle for port applications. Specifically, this work aims at laying the foundations for the development of a benchmark industrial cargo–handling hydrogen-fueled vehicle to be used in real port operations. To this purpose, an on-field measurement campaign has been conducted to analyze the duty cycle of a commercial Diesel-engine yard truck currently used for terminal ports operations. The vehicle dynamics has been numerically modeled and validated against the acquired data, and the energy and power requirements for a plug-in fuel cell/battery hybrid powertrain replacing the Diesel powertrain on the same vehicle have been evaluated. Finally, a preliminary design of the new powertrain and a rule-based energy management strategy have been proposed, and the electric energy and hydrogen consumptions required to achieve the target driving range for roll-on and roll-off operations have been estimated.

The results are promising, showing that the hybrid electric vehicle is capable of achieving excellent energy performances, by means of an efficient use of the fuel cell. An overall amount of roughly 12 kg of hydrogen is estimated to be required to accomplish the most demanding port operation, and meet the target of 6 h of continuous operation. Also, the vehicle powertrain ensures an adequate all-electric range, which is between approximately 1 and 2 h depending on the specific port operation.

Potentially, the hydrogen-fueled yard truck is expected to lead to several benefits, such as local zero emissions, powertrain noise elimination, reduction of the vehicle maintenance costs, improving of the energy management, and increasing of operational efficiency.

1. Introduction

The maritime transport sector has an essential role in the international trade and global economy. However, it is a large and growing source of greenhouse gas (GHG) emissions. Currently, the CO_2 emissions from shipping are estimated around 1 billion tons per year, which represent about the 2.5% of global GHG emissions [1]. The impact of shipping at European Union (EU) level is also considerable, with its associated emissions representing the 13% of the overall GHG emissions from the transport sector [1]. According to projections [2], CO_2 emissions from maritime transport are likely to undertake a significant increase in the future: at least 50% by 2050, even in the most optimistic scenario. In this context, the overall shipping emissions in seaports, that are the emissions caused by and related to ships port stays, represent a not negligible share. These are indeed substantial, accounting for roughly 20 million tons of CO_2, as well as for considerable amounts of NO_x, SO_x and PM_{10} [3–5]. In line with the trend of the whole maritime sector, in-ports emissions show a tendency to grow significantly in the

* Corresponding author.
E-mail address: giovanni.diilio@uniparthenope.it (G. Di Ilio).

https://doi.org/10.1016/j.enconman.2021.114423
Received 1 March 2021; Accepted 13 June 2021
Available online 30 June 2021

near future, with around 70 million tons of CO_2 and 1.3 million tons of NO_x being the estimated values in 2050 [5]. This scenario urgently calls for a reinforcement of the harmful emissions reduction efforts.

Despite most of the shipping emissions take place during the actual transport by sea, those from in-port operations have the most noticeable environmental impact at local scale. Port facilities are indeed typically located near cities or residential areas, thus affecting directly the air and water quality of urban environment. Also, port infrastructures, services and related equipment, have achieved a significant technological development in recent years. Such advances have provided remarkable benefits in terms of port operations capabilities, but still inefficiencies remain, resulting in large energy consumption which negatively affect the environment. As for other sectors, the pathway to achieve deep decarbonisation and mitigation of energy use in the maritime transport and, more specifically, in the port-logistic industry, encompasses and requires multiple combined options [6]. These include: i) the use of alternative fuel sources [7–9] and ii) of advanced propulsion systems for vessels [10,11], especially based on fuel cells [12,13], iii) the reduction of the vessel Diesel engines emissions by means of innovative technologies [14], iv) the rationalization of ports energy demands, v) the adoption of specific strategies to provide power to the ship at berth from an external source (i.e. cold ironing) [15], as well as vi) the application of renewable energy technologies in port operations [16–18]. All of these actions aim at driving the port industry toward a more sustainable future. However, to date, there is still a significant untapped potential to reduce emissions and meet the stringent regulatory requirements for urban air quality.

The high environmental impact from ports is mainly due to two aspects. The first one is related to the considerable energy consumption of vessels at berth during port stays, which is generated by their large auxiliary engines. This consumption is required to feed accessory systems such as those for heating, ventilation, and lighting, as well as to support all the necessary cargo operations. A second but still relevant aspect is instead related to the vast number of machinery, vehicles and cranes required for port operations. The road transport within port areas by means of yard trucks, forklifts, container movers, rubber tired gantry cranes and material handling vehicles of different kind represents indeed a major source of emissions in ports. The use of these vehicles, when powered by fossil fuel, not only contributes to port emissions by direct fuel consumption, but also leads to a significant increase of the vessel energy demand, since it induces some of the on-board auxiliary systems to operate intensively. This is especially the case of the ventilation system, which is required to operate to avoid a build up of the pollutants produced by the vehicles engines, which are harmful to the health of workers on the ship. Hence, in order to comply with emissions requirements and to facilitate the transition of existing port terminals towards effective low-carbon/zero-emissions areas, heavy-duty vehicles for port operations must be redesigned [19]. Achieving zero local emissions power solutions for large-size freight vehicles at seaports is however an ambitious challenge. In fact, the need for a continuous and long-lasting operation (i.e. very low refueling/recharging times allowed) as well as the inherently high power demand require a considerable amount of both energy to be stored on-board and available power. Also, the wide variability of operating conditions and tasks characterizing typical Roll-on/Roll-off (RoRo) duty cycle for these vehicles represents a crucial aspect. These, among other technical limitations, are all factors which have obstructed the process of electrification for port-logistic vehicles until now.

In the pursuit of higher energy efficiency and reduction of harmful emissions, hydrogen Fuel Cell (FC) technologies represent a promising and viable solution in transportation [20,21], for a wide class of vehicles and applications, including light [22,23] as well as medium [24,25] and heavy-duty [26–30]. This especially applies to the logistic road transport [31,32] and, potentially, to the port sector, where FCs may help to cope with several issues. In fact, besides being inherently clean, FC technologies own many favorable features, such as scalability, flexibility, high efficiency and silence, which may bring significant advantages in several port operations. Moreover, their use in hybrid electric architectures is instrumental to extend the driving range of the vehicle and reduce recharging times. For these reasons, hydrogen FCs have attracted great interest from port industry, even though the first actual experiences are yet in their infancy.

Several works in literature deal with the implementation of hybrid electric powertrain solutions based on FCs in heavy-duty vehicle applications, but none of them is oriented to the port-logistic sector. Within this framework, the aim of the present work is to propose a preliminary design of a hydrogen fuel cell/battery hybrid powertrain for a zero-emissions heavy-duty port Yard Truck (YT), today widely used, in its conventional Diesel engine configuration, for RoRo operations by the major port operators worldwide. Specifically, the powertrain design proposed in this study is based on real terminal port operations: an on-field measurement campaign has been carried out to acquire a typical duty cycle for a YT vehicle, serving a cargo ship, during normal RoRo operations. The Diesel–fueled vehicle dynamics was then numerically modeled and validated against on-field acquired data, and its energy performance was analyzed, in such a way to define the energy and power requirements for the hybrid electric powertrain. This allows sizing and selecting the main powertrain components for the new hydrogen fueled vehicle, that are electric motor, battery pack and FC. Finally, the hydrogen fueled vehicle energy performance are assessed and the hydrogen fuel consumption required to achieve the target driving range is estimated, implementing a rule-based energy control strategy. The numerical modeling of the vehicle dynamics and of its energy management is realized through the use of MATLAB software, by means of an ad hoc developed code. The intent behind this research is to provide a first significant step to the successful introduction of FC industrial vehicles inside the port sector, towards a zero-emissions vehicle (ZEV) fleets scenario.

2. ICE vehicle description and operation

The new hydrogen fueled vehicle has been developed starting from a Terberg RT223 YT, which is a 4x4 heavy-duty yard tractor used in ports logistic, and in particular in RoRo operations of trailers on ships. The vehicle weight is around 11.5 t and it is powered by a Volvo TAD871VE Diesel engine of 7.7 dm^3 displacement with 185 kW of maximum power. The powershift transmission has 6 speeds forward and 3 speeds reverse. Table 1 reports the main characteristics of the Terberg RT223 YT vehicle, while Fig. 1 shows a schematic representation of the vehicle powertrain architecture. During Roll-on operation, the YT drives a wheeled cargo (often a trailer) from the on-shore terminal to the ship. Within the vessel, the YT climbs one or more internal ramps while being fully loaded. This represents the most demanding stage of the whole

Table 1
Terberg R223 YT technical specifications [33].

Engine			**Volvo TAD871VE**			
Displacement			7.7 dm^3			
Compression ratio			17.5:1			
Power			185 kW @ 2200 rpm			
Torque			1160 Nm @ 1000–1400 rpm			
Gearbox			**ZF, type 6WG211**			
Forw. gear-shift	1st	2nd	3rd	4th	5th	6th
Gear ratio	5.683	3.702	2.304	1.501	0.963	0.627
Rev. gear-shift	1st	2nd	3rd			
Gear ratio	5.041	2.044	0.854			
Transfer case			**Kessler, type W1000**			
Reduction ratio			1.371:1			
Front/Rear axle			**Kessler**			
Reduction ratio			16.3:1			
Tires			11R22.5			
Rims			10 stud disc wheels 22.5 x 8.25			

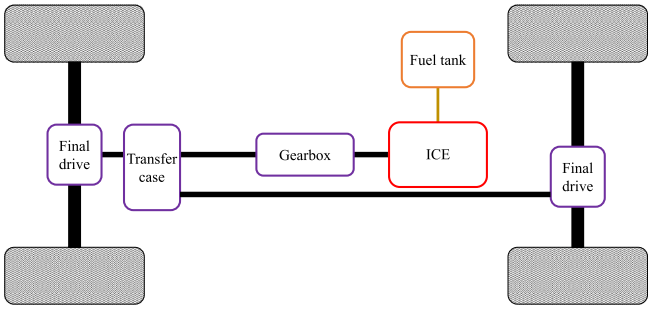

Fig. 1. Schematic representation of the ICE vehicle configuration.

operation, in terms of required power. At this point, the vehicle releases the trailer and comes back unloaded to the terminal area. On the contrary, during Roll-off operation, the YT enters the ship and climbs the internal ramps with no load. After loading, it drives off the ship the trailer, thus climbing the internal ramps down while carrying the full load. Both the described operations take around 10 min to be completed, and they must be repeated continuously for a total time of 6 h.

3. ICE vehicle data acquisition

The new hybrid electric powertrain design is grounded on real operation data. An accurate and realistic representation of typical duty cycles is indeed crucial to properly model the vehicle dynamics and evaluate the energy and power output demands. Therefore, an on-field measurement campaign was conducted at the Grimaldi's Terminal located in port of Salerno, Italy.

In particular, several data acquisitions were performed during normal Roll-on and Roll-off operations of the vehicle, directly accessing the internal combustion Engine Control Unit (ECU) as well as the Transmission Control Unit (TCU). Specifically, among other quantities, the profiles of engine torque, engine rotational speed and fuel consumption were acquired from the ECU. Instead, vehicle speed profile, driveshaft rotational speed and engaged gear were retrieved from the TCU. Note that data sampling rates were different among ECU and TCU, with the former being constant and equal to 4 Hz, while the latter being variable and ranging between 9 and 11 Hz. Such a mismatch was overcome by performing a time synchronization of data by means of linear interpolation during post-processing. Both Roll-on and Roll-off data acquisitions were performed on the same day, from two different cargo ships (one arriving and one leaving), of the same kind and of identical configuration.

Several Roll-on and Roll-off cycles were acquired during the measurement campaign, among which only one for each kind of operation was selected as a reference cycle. It is worth emphasizing that the two reference cycles were selected after assessing their consistency (i.e. absence of spurious events, such as delayed operation due to unexpected traffic conditions) rather than on a statistical analysis, since this would have led to unrealistic cycles, due to the inherent high variability of the real driving conditions. The chosen reference Roll-on cycle has an overall duration of 600 s, while the Roll-off one is slightly shorter, with an overall duration of 540 s. Also, the measured fuel consumption related to the considered reference duty cycles are of 1.64 kg and 1.10 kg for Roll-on and Roll-off, respectively, which lead to 59.2 kg and 44.0 kg of fuel consumed over 6 h of continuous operation (i.e. target time of operation).

During the Roll-on operation monitored and used for our data acquisition, the YT towed a trailer from the terminal area to the second deck of the cargo ship. The slope of the internal ramps is 10.5% (i.e. 6^{o}), as reported by the ship technical drawing. The weight of the trailer towed during data acquisition was estimated to be about 30 t by the transport company that owned the trailer. Conversely, during the considered Roll-off operation, the trailer was towed from the second deck of the cargo ship to the terminal area. Also in this case, the slope of the ramps inside the ship is 10.5%. However, differently from Roll-on, the weight of the trailers was 15 t, as estimated by the transport company. The stages that compose the Roll-on and Roll-off reference cycles are listed and described in detail in Tables 2 and 3, respectively. A ground operator was able to note precisely the start and the end of each phase of the mission, so that it was then possible to reproduce slope and vehicle mass profiles (including the trailer), as reported in Figs. 2 and 3, respectively.

3.1. Driving cycles

As already mentioned, the speed profiles for typical Roll-on and Roll-off operations have been acquired during the on-field measurement campaign. However, in order to develop suitable reference driving cycles for the numerical simulation of the vehicle dynamics, the acquired data were post-processed, as here described.

The modeling of the vehicle dynamics requires indeed the computation of the vehicle acceleration, i.e. the speed derivative in time. Due to the resolution of the speed sensor module of the TCU, the recorded speed profile results to be a piecewise step function. The mathematical nature of such a speed function does not allow an accurate representation of the vehicle acceleration, since the error-prone numerical discretization of the speed derivative in time would unavoidably lead to an unrealistic acceleration profile. Therefore, to cope with this issue, a simple yet effective smoothing procedure was implemented to obtain a more convenient function for the vehicle speed.

To this aim, the vehicle speed at new time instants, that is, every 0.25 s (i.e. ECU sampling rate) is first computed by means of linear interpolation, in order to synchronize the speed profile with data from ECU. The speed function is then smoothed out by performing a moving average, that is each element of the new speed function is computed as the mean over a sliding window of certain length across the neighboring elements. The length of such a sliding window is a key parameter, since it significantly affects the accuracy of the results. Thus, after performing a sensitivity analysis for such a parameter, a sliding window of 2 s is selected. Afterwards, the acceleration profile is computed by means of a central finite difference scheme for the time derivative of the velocity. To further alleviate spurious acceleration peaks, a moving average for the acceleration function is performed as well, with again a sliding window of 2 s. The so obtained profile, which is shown in Fig. 4 for both the YT operations, is suitable to be implemented into the vehicle dynamics model. Finally, the vehicle speed profile is updated by integrating the computed acceleration function. The obtained vehicle speed profiles, in comparison with the original acquired data, are shown in Figs. 5 and 6, for Roll-on and Roll-off operations, respectively. The results presented in Figs. 5 and 6 prove the accuracy of the implemented smoothing procedure: the post-processed vehicle speed profiles fairly match the ones acquired from the TCU, thus they have been used as reference driving cycles in this work.

Also, Fig. 7 presents the speed frequency distributions related to the

Table 2
YT operations for the Roll-on reference cycle.

N.	YT Roll-on operations
1	loading the trailer in the on-shore terminal area
2	carrying the trailer from the on-shore terminal into the ship
3	climbing ramp #1 to reach the first deck
4	driving inside the ship
5	climbing ramp #2 to reach the second deck
6	driving inside the ship
7	unloading the trailer
8	driving inside the ship
9	climbing down ramp #2
10	driving inside the ship
11	climbing down ramp #1
12	return to the on-shore terminal area

Table 3
YT operations for the Roll-off reference cycle.

N.	YT Roll-off operations
1	driving with no trailer from the on-shore terminal into the ship
2	climbing ramp #1 to reach the first deck
3	driving inside the ship
4	climbing ramp #2 to reach the second deck
5	driving inside the ship
6	loading the trailer
7	driving inside the ship
8	climbing down ramp #2
9	driving inside the ship
10	climbing down ramp #1
11	return to the on-shore terminal area
12	unloading the trailer

two reference driving cycles. The two speed frequency distributions are similar one to the other: for almost half of the time of operation, the vehicle speed is lower than 5 km/h, while its peak speed is about 30 km/h for both Roll-on and Roll-off operations.

4. Vehicle dynamics modeling and validation

To design the hybrid electric vehicle (HEV) powertrain, a model of the vehicle longitudinal dynamics is first derived and then validated by comparing the estimated power requested to the ICE by the reference driving cycle with the ICE power retrieved from the ECU during data acquisition. The signal inputs to the HEV powertrain will be then predicted by using a quasi-static backward approach, which makes use of the developed vehicle dynamics model along with the predetermined driving cycle. The accurate estimation of the output power profile as well as of the energy consumption are crucial for the sizing of battery and FC module of the HEV.

According to the dynamic equation of motion along the longitudinal direction, the total tractive effort F_t of the vehicle reads as follows:

$$F_t = F_r + \delta m_v a \tag{1}$$

where m_v is the vehicle mass, a is the instantaneous acceleration, δ is the mass factor, that is a coefficient accounting for the equivalent mass increase due to the angular moments of the rotating components of the vehicle, and F_r is the total resistance force. The vehicle resistance F_r includes three contributions, namely aerodynamic drag, rolling resistance of tires and grading resistance. By writing in an explicit way each of these terms, it results:

$$F_r = \frac{1}{2}\rho v^2 A C_d + f_r m_v g\cos\theta + m_v g\sin\theta \tag{2}$$

where ρ is the air density, v is the vehicle speed, A is the vehicle frontal area, C_d is the aerodynamic drag coefficient, f_r is the rolling resistance coefficient, g is the gravity acceleration, and θ is the road angle. The vehicle mass and road slope vary along the traveled path, thus they are a function of time, as detailed in the previous Section, see Figs. 2 and 3. Also the rolling resistance coefficient is taken as a variable parameter in our model, in order to take into account the high heterogeneity of the

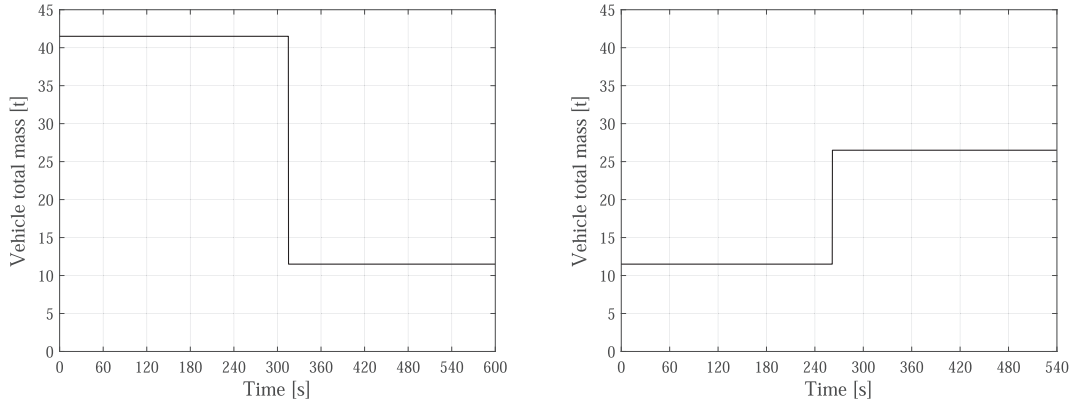

Fig. 2. Acquired vehicle mass profiles during the reference Roll-on (a) and Roll-off (b) operations.

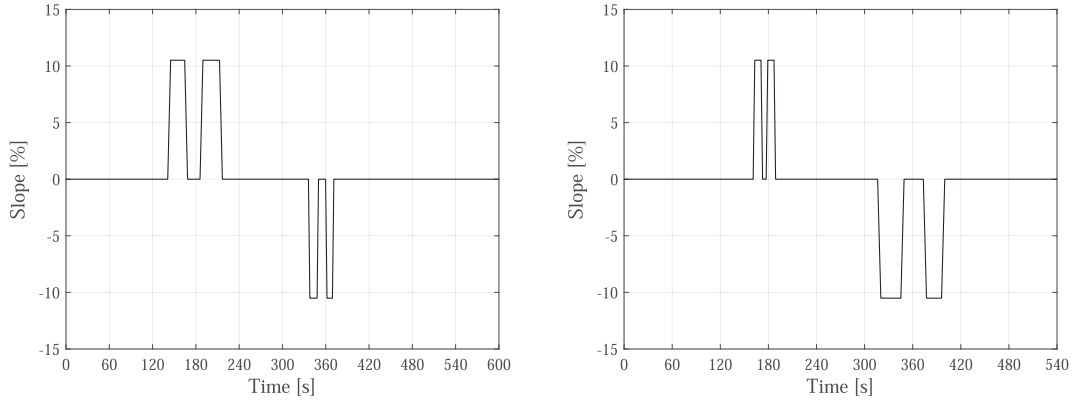

Fig. 3. Acquired slope profiles during the reference Roll-on (a) and Roll-off (b) operations.

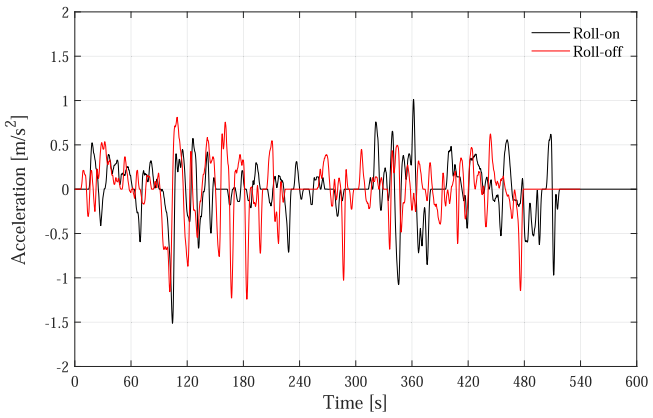

Fig. 4. Vehicle acceleration profiles for the reference Roll-on and Roll-off driving cycles.

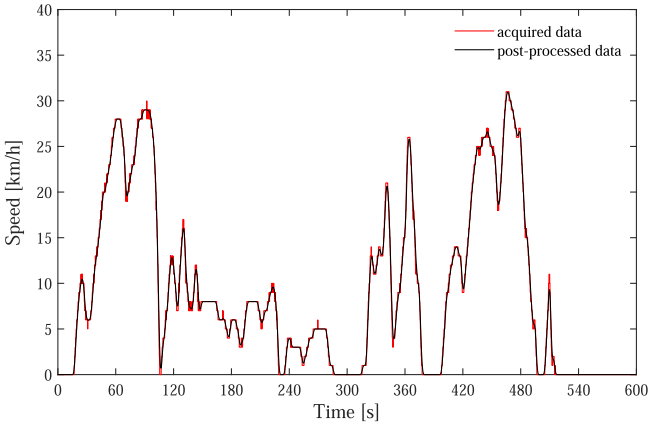

Fig. 5. Reference driving cycle: vehicle speed profile during a typical Roll-on operation.

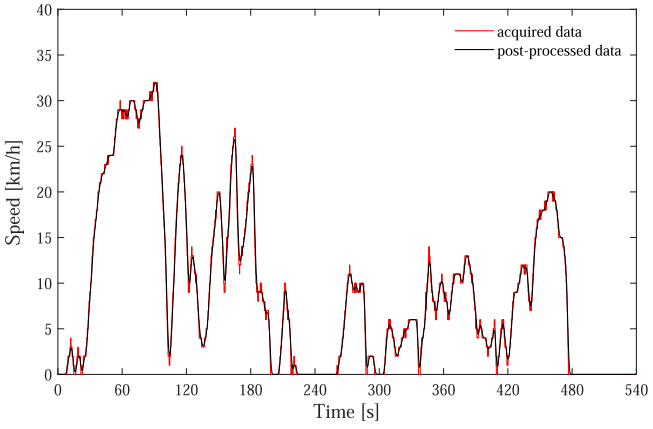

Fig. 6. Reference driving cycle: vehicle speed profile during a typical Roll-off operation.

road, and also the varying weight of the vehicle over the mission. Table 4 reports all the values set for the model parameters in Eqs. (1) and (2). The mechanical power P_w that has to be provided to the wheels of the vehicle is computed as:

$$P_w = F_t v \tag{3}$$

Finally, the power request at the ICE is estimated by taking into account the overall drivetrain losses as well as the auxiliary loads, as per the following equation:

$$P_{\mathrm{ICE}} = \frac{P_{w_+}}{\eta_t} + P_{aux} \tag{4}$$

where P_{w_+} indicates the power related to the positive tractive force, that is: $P_{w_+} = P_w$ for $P_w > 0$, and $P_{w_+} = 0$ otherwise. The power P_{aux} requested by the auxiliaries, including water pump, cooling fan, air compressor and oil pump, amounts up to roughly 5 kW during the mission, as acquired from the ECU. The term η_t in Eq. (4) represents instead the total mechanical efficiency of the vehicle transmission between the engine output shaft and the drive wheels. This is computed by considering an efficiency of 0.96 for each of the transmission components, that are a longitudinal differential and a planetary wheel for front/rear axle, as well as for each engaged pair of gears in the gearbox. The product of all the efficiencies for the named elements of the driveline leads to a value of η_t ranging between 0.78 and 0.85 depending on the used gear-shift, which are in line with the average values for the transmission efficiency of heavy-duty vehicles [34]. Table 5 reports the number of engaged pairs of gears (EPG) for each gear-shift, as reported in the vehicle technical specification manual. It is worth emphasizing that reverse gears are used for backing maneuvers needed to place the truck in the correct position when loading/unloading the trailer, but they are also used, in general, to climb the internal ramps of the ship when the truck carries very heavy loads: in this case the truck drives in reverse for stability reasons. The latter is a common strategy which has not been adopted, however, during the RoRo operations acquired in the present study, where ramps are climbed up always in forward mode. Figs. 8 and 9 show the calculated power profiles for the ICE vehicle resulting from simulation, in comparison with the on-board measurements, for the two reference driving cycles, namely single Roll-on and Roll-off operations, respectively. The results shown in Figs. 8 and 9 are satisfactory, with a good agreement observed between the measured and the computed duty cycles. Overall, the numerically predicted power demands at ICE follow well the expected profiles, with some differences mainly due to the inherent approximation of some of the model parameters. However, such minor discrepancies can be considered acceptable to the aim of the present work, since they do not affect the overall vehicle performance. As expected, the Roll-on is the most energy and power demanding operation among the two considered, as can be clearly noted by observing the duty cycles reported in Figs.8 and 9. Thus, in order to make the HEV capable of achieving the most critical conditions, in terms of peak power and on-board energy availability, its powertrain is designed based on the Roll-on operation duty cycle. The measured maximum and mean powers requested to the ICE of the vehicle, along with its overall energy consumption, during Roll-on and Roll-off operations, in comparison with those estimated by means of our model, are reported in Table 6. The obtained values of maximum and mean power outputs are in line with the corresponding ones taken from the ECU. In particular, the results show that the mean power demand for the Roll-on operation is about 50% higher than that for Roll-off operation. Also the computed overall energy demand for the vehicle is in fair agreement with the one expected from the acquisitions, which have been computed by integrating the real power profiles, known from the ECU, over the time.

5. HEV performance analysis

The first step of the analysis concerns the determination of the overall required electric power that has to be supplied by battery and FC to the traction electric motor (EM), as well as the determination of its operating points, in terms of output torque and speed. The considered EM is the Danfoss EM-PMI375-T1100 [38]. This is a permanent magnet machine, allowing for a maximum peak torque of 2100 Nm at 350 A, when driven by a single inverter, and a maximum peak torque of 3270 Nm in its double inverter configuration. The maximum continuous

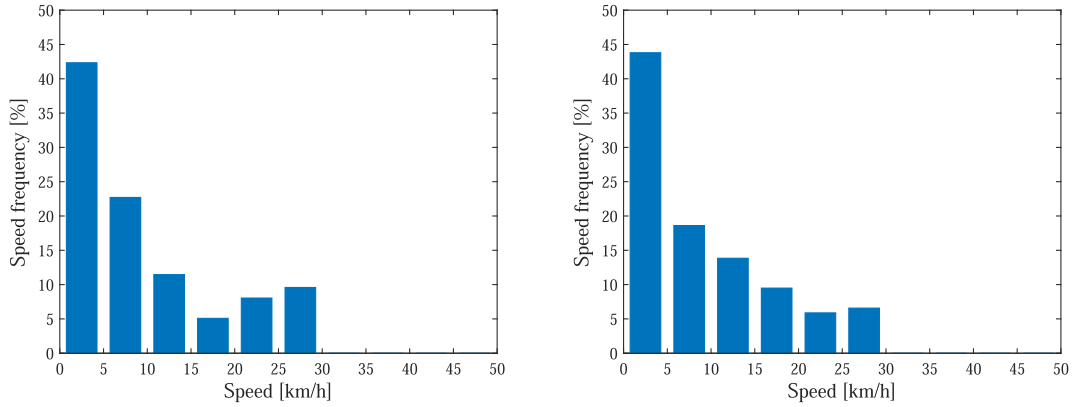

Fig. 7. Speed frequency distribution for the reference driving cycles related to Roll-on (a) and Roll-off (b) operations.

Table 4
Vehicle longitudinal dynamics model parameters.

Parameter	Value
A	8 m^2
C_d	0.8
f_r	0.015–0.065 [34,35]
ρ	1.2 kg/m^3
δ	1.1 [36,37]

Table 5
Number of engaged pairs of gears for each gear-shift [33].

	Forward						Reverse		
Gear-shift	1st	2nd	3rd	4th	5th	6th	1st	2nd	3rd
N. of EPG	3	3	3	4	3	4	4	2	2

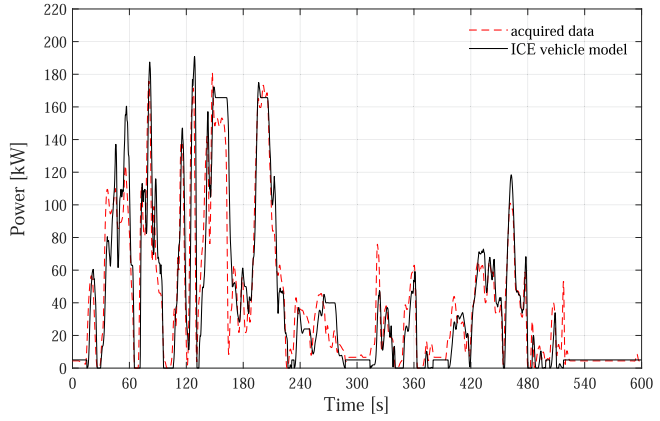

Fig. 8. ICE power demand as a function of time for the reference Roll-on driving cycle.

torque that can be delivered by the motor is 1515 Nm. Its peak efficiency is about 0.96.

With the power demand at the wheels known from the vehicle dynamics model, the electric power required at the EM is given by:

$$\begin{cases} P_{EM} = P_w/\eta_t', & \text{if} \quad P_w \geqslant 0 \\ P_{EM} = P_w\eta_t', & \text{if} \quad P_w < 0 \end{cases} \tag{5}$$

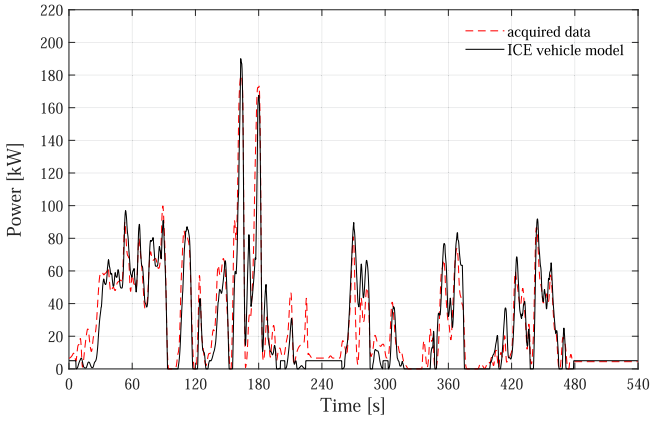

Fig. 9. ICE power demand as a function of time for the reference Roll-off driving cycle.

Table 6
Mean and maximum power and overall energy consumption at the ICE output shaft for the original vehicle as computed by the numerical model and from acquired data.

	numerical model			acquired data		
	$P_{ICE_{mean}}$	$P_{ICE_{max}}$	$E_{ICE_{tot}}$	$P_{ICE_{mean}}$	$P_{ICE_{max}}$	$E_{ICE_{tot}}$
	[kW]	[kW]	[kWh]	[kW]	[kW]	[kWh]
Roll-on	40.0	190.8	6.67	40.0	181.0	6.67
Roll-off	25.7	190.0	3.85	27.5	179.7	4.13

where the second equation takes into account the regenerative braking, that is the negative mechanical power at the wheels (i.e. the braking power) that can be converted into electrical energy to be stored in the battery. In the present study, the assumption is made that the 100% of the available braking power is recovered. The term η_t' in Eq. (5) indicates the overall transmission efficiency of the HEV driveline, which differs from the one computed for the ICE vehicle. In fact, for the HEV configuration analyzed in this work, a direct drive mechanism is assumed (i.e. no gearbox is used). This is possible thanks to the EM characteristics and would allow to better accommodate the hydrogen tanks and the EM in the engine bay, in principle. The parameter η_t' is therefore calculated as the product of the efficiencies of the two main components of the drivetrain, namely the longitudinal differential and the planetary wheel at front/rear axle, which leads to a constant value of

0.92.

In order to retrieve the instantaneous efficiency of the EM and to assess its actual capability of providing the required power, the EM speed and torque profiles, as a function of the vehicle speed, must be evaluated. These are computed as follows:

$$n_{EM} = n_w i_0 \tag{6}$$

$$T_{EM} = \frac{60 P_{EM}}{2\pi n_{EM}} \tag{7}$$

where $i_0 = 22.3$ is the overall gear ratio (Table 1) and n_w is the rotational speed of the vehicle wheels, which is given by:

$$n_w = \frac{60v}{\pi D} \tag{8}$$

with D being the wheel diameter ($\sim$ 1 m, [33]). The EM operating points given by the computed torque-speed pairs fall within the EM regular working area, for either the Roll-on and the Roll-off operations, as presented in Figs. 10 and 11. The determination of the EM operating points allows evaluating the EM efficiency profile η_{EM}, which is retrieved from the available map. The resulting mean efficiency for the EM is roughly equal to 0.93 for both the YT operations. This value further confirms that the selected EM, along with the choice of not including a gearbox in the HEV drivetrain, can be considered a suitable option.

Finally, the total electric power requested to the HEV FC/battery unit is computed as follows:

$$\begin{cases} P_{tot} = P_{EM}/\eta_{EM} + P_{aux}, & \text{if} \quad P_{EM} \geqslant 0 \\ P_{tot} = P_{EM}\eta_{EM} + P_{aux}, & \text{if} \quad P_{EM} < 0 \end{cases} \tag{9}$$

The calculated profiles of P_{tot} for the reference Roll-on and Roll-off driving cycles are shown in Figs. 12 and 13, respectively, where the RoRo operations timeline is also reported as per Tables 2 and Tables 3. Table 7 reports the obtained maximum and mean power output as well as the overall energy that the HEV FC/battery unit must provide, for each reference operation. As expected, the Roll-off operation requires lower power and energy outputs with respect to the Roll-on operation. However, the HEV powertrain demands for both the operations are significantly lower than the corresponding ones for the ICE vehicle, because of both the higher overall efficiency of the hybrid driveline (i.e. the absence of the gearbox) and the regenerative braking, which is considered in the computed values.

6. HEV powertrain design

The proposed HEV is designed as a plug-in vehicle, and a schematic representation of its powertrain architecture is represented in Fig. 14. The HEV power unit should integrate all the main components shown in Fig. 14 in such a way to fulfill at least the same energy performance of the Diesel engine power unit. In particular, the FC module should be able to provide the requested mean power, while the battery pack should be able to fulfill the power spikes during critical acceleration events and to recover energy when braking. This hybrid architecture allows for

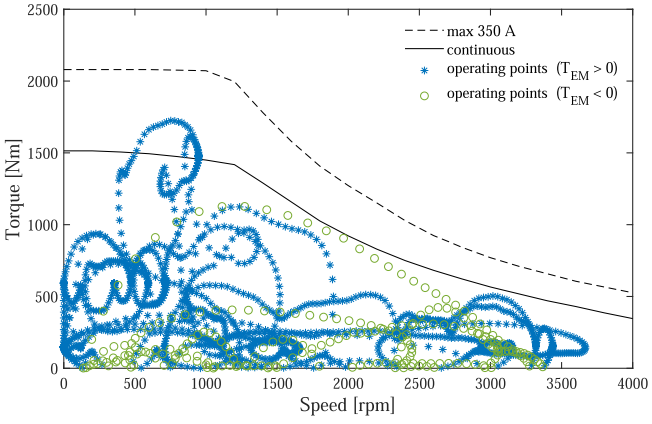

Fig. 10. EM output operating points in the torque-speed plane, for the Roll-on reference driving cycle.

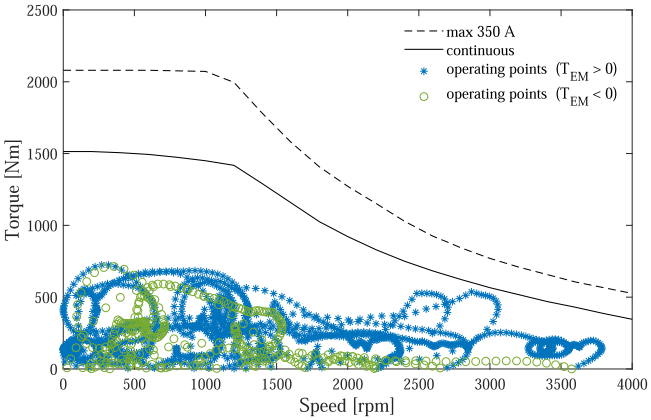

Fig. 11. EM output operating points in the torque-speed plane, for the Roll-off reference driving cycle.

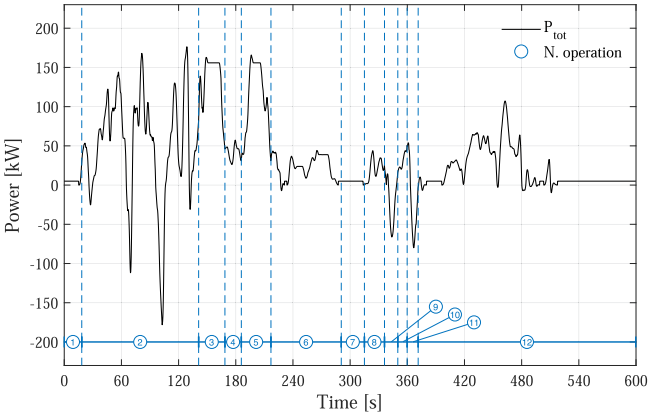

Fig. 12. HEV power demand as a function of time for the Roll-on reference driving cycle. Numbered circles represent the YT operations as described in Table 2.

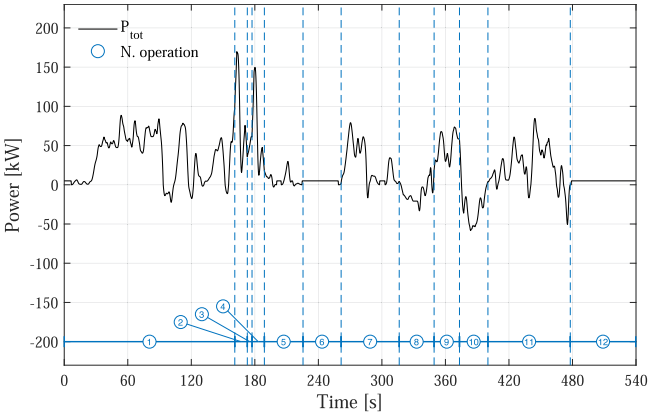

Fig. 13. HEV power demand as a function of time for the Roll-off reference driving cycle. Numbered circles represent the YT operations as described in Table 3.

Table 7
Mean power, maximum power and energy consumption at FC/battery output for the HEV performing single Roll-on and Roll-off reference operations.

	$P_{tot_{mean}}$ [kW]	$P_{tot_{max}}$ [kW]	E_{tot} [kWh]
Roll-on	34.0	176.3	5.67
Roll-off	20.9	169.7	3.14

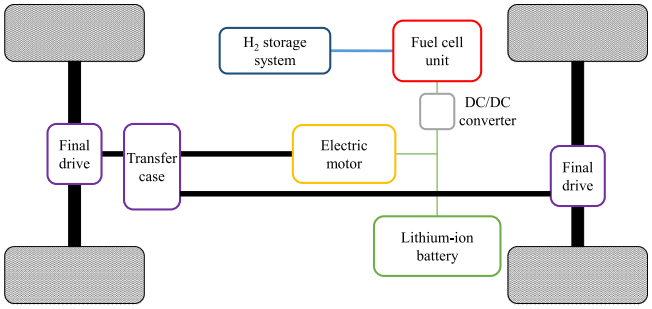

Fig. 14. Schematic representation of the proposed HEV configuration.

components downsizing, thus reducing costs and total weight. According to the scheme in Fig. 14, the FC unit, which is connected via a DC/DC converter to the high voltage bus and, in turn, to the battery pack and the motor inverter, either supplies electric power to the EM, recharges the battery, or accomplishes both tasks simultaneously. Thus, the EM can be powered either by the FC, the battery, or both at the same time.

The hydrogen-powered vehicle has to accomplish the same tasks and ensure the same operation capability of the Diesel engine vehicle. This means that the new fuel cell/battery hybrid power unit should be able to deliver at least the same power requested at wheels as for the ICE vehicle, while the electric drivetrain should deliver the same requested torque and speed. Moreover, the vehicle's range of operation has to guarantee at least one 6 h shift of continuous operation before refueling and recharging. Based on these constraints, and by considering the estimated power profile requested at the EM for the most demanding YT operation (i.e. Roll-on), the main specifications of the HEV powertrain components are defined and provided in the following.

6.1. Battery pack

The battery pack in the hybrid power unit has to i) provide power to the vehicle during transient operations: the battery pack should be sized on the maximum power required by the EM, ii) recover kinetic energy during braking: the battery pack should be verified considering the maximum allowed charging C-rate from regenerative braking, and iii) ensure an adequate all-electric range: the battery pack should store enough energy to carry out the ongoing task and drive the vehicle into the maintenance box in case of a FC system failure.

In this study, a $LiFePO_4$) chemistry is considered for the battery pack, given its higher cycling and thermal stability features, when compared to other battery chemistries [23,39]. In line with typical data for such a technology, and in order not to stress the battery, thus avoiding its premature wear, the battery maximum peak discharge C-rate is taken equal to 5C, while the maximum continuous discharge rate is 3C. As for charging, the maximum peak C-rate is taken equal to 1.5C, while the maximum continuous charge C-rate is 1C. Table 8 summarizes such assumed values. The maximum continuous charging C-rate is expected to be reached when the battery pack is charged by the FC stack and the vehicle is not in motion, while the peak charging C-rate is likely to occur during regenerative braking. When the regenerative power exceeds the maximum peak charging power, the mechanical brake kicks in and the kinetic energy is dissipated. The recovery of the kinetic energy is a key factor in the battery pack sizing, especially considering that the net

Table 8
Continuous and peak C-rate for battery charge and discharge.

	Continuous	Peak
Battery discharge	3C	5C
Battery charge	1C	1.5C

amount of energy that can be potentially recovered from braking is equal to the 9.3% and 12.5% of the total tractive energy required to the FC/battery unit, for Roll-on and Roll-off operations, respectively, as estimated by our model. In general, the most significant regenerative braking events occur during the descent of the ramps. As such, the maximum share of kinetic energy that can be theoretically recovered is higher for the Roll-off operation since, in this case, the YT tows the loaded trailer during the descent of the ramps. In contrast, the YT carries no trailer when climbing down the ramps during Roll-on operation, thus the regenerative braking events are in this case less relevant. On the light of this, the battery capacity is set in such a way to maximize the amount of recovered energy, while making a trade-off with its sizing. To this purpose, a parametric analysis was performed on both Roll-on and Roll-off duty cycles to evaluate the maximum share of kinetic energy that can be actually recovered, over the total available, depending on the installed battery capacity, as represented by the percentage parameter E_{rb} portrayed in Fig. 15. For a given battery capacity, the maximum share of kinetic energy that can be actually recovered during the Roll-on operation is even reduced, since the regenerative braking events occurring during the Roll-on operation are characterized by higher peaks of power, which may exceed the peak charging power allowed by the battery. With an overall battery capacity of 60 kWh, the energy storage system is capable of recovering the whole share of available kinetic energy during braking events in Roll-off operation, and more than the 85% in Roll-on operation. This is a sufficient share in order to maximize the energy recovery without oversizing the battery pack. Thus, 60 kWh is the nominal battery capacity that is considered in our design.

6.2. Fuel cell stack

In principle, the FC stack in the hybrid power unit has to provide the requested mean power in order to avoid the battery State of Charge (SoC) depletion under continuous vehicle operation. Therefore, the FC rated power could be selected by considering the mean power requested during the most demanding operation, as detected from the duty cycle analysis (i.e. 34.0 kW during Roll-on operation). However, the

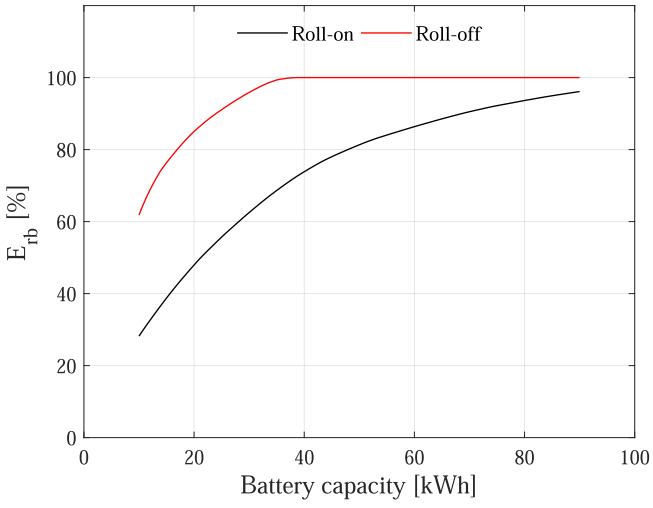

Fig. 15. Percentage of kinetic energy that can be recovered as a function of the battery capacity, for Roll-on and Roll-off operations.

considered port operations are subject to high variability, in terms of real driving conditions. There are indeed several peculiar factors that may highly influence the RoRo duty cycles, such as auxiliary power during stops required to load and unload the trailers, mean speed constraints, driving skills of the driver, variable weight of the trailers, and variable slope of the ramps along the path. All of these represent key aspects which may affect substantially the power demand of the vehicle, in real operation. For this reason, the FC stack rated power must be actually oversized with respect to the mean power demand for the reference Roll-on duty cycle. The selected FC module is the Ballard FCmove™-HD 70 kW [40], which is specifically designed for transit buses, medium and heavy duty trucks, and rail applications. As will be detailed in Section 7, such a maximum power output matches well with the energy requirements of the selected battery pack during its charging. The chosen FC module is characterized by an overall high efficiency in the desired range of operation, with a peak efficiency of 57%. Moreover, its size fits well with the space availability on the YT vehicle under consideration.

7. HEV energy management

In general, the energy management of a HEV can be addressed by means of several strategies [41,42]. These include the adoption of rule-based as well as optimal approaches. In particular, optimal control strategies, such as those based on Dynamic Programming or the Pontryagin's Minimum Principle [43,44], are aimed at minimizing the fuel consumption over a given driving cycle, while ensuring the fulfillment of power request at the wheels of the vehicle. Nonetheless, their implementation requires the a priori knowledge of the driving cycle, thus these algorithms cannot be always applied for on-line energy management. Moreover, the fuel cell power profiles always resulted in being similar among different controllers based on different algorithms [37,45–47]. In particular, since the fuel cell is characterized by an efficiency monotonically decreasing with the increasing of the load, when used, it is run at a partial load, corresponding to the maximum efficiency, and the use at full load is avoided. For this reason, an in-depth study on the optimal energy management of the vehicle is left to subsequent steps of this research, while in this work a simplified rule-based control strategy is implemented, based on a feedback control on the battery SoC. In particular, a Charge Depleting/Charge Sustaining (CD/CS) strategy is employed, where the vehicle is firstly run as a Battery Electric Vehicle (BEV) and then, only when the battery charge is depleted, it operates as a charge sustaining HEV with the fuel cell running at partial load. The key advantage of such an energy management strategy lies in its robustness and reliability and inherent ease of implementation, being the knowledge of the driving cycle not required a priori. These aspects, make it particularly suitable for a preliminary estimation of the energy performance for the proposed powertrain solution.

The control algorithm for the implemented energy management strategy reads as follows:

1. At the initial state, the battery is supposed to be almost fully charged, that is, the initial SoC is set to 90%. This value, despite being chosen arbitrarily, may be considered as representative of realistic conditions: the vehicle continuously operates for a 6 h shift per day, therefore, there is sufficient time, during its stops, to recharge the battery from the electric grid. Thus, initially, the vehicle operates as a BEV, i.e. the EM draws energy only from the battery, while the FC is switched off (CD mode of operation). During this stage, the battery is discharged until its SoC reaches a predefined limit value, which is set equal to 30%. With the occurring of this event, the powertrain operation switches to the hereafter referred to as Charging Mode (CM).
2. In CM, the FC starts to operate as primary energy source to supply power to the EM and to recharge the battery. In particular, the FC power is set to a constant value, close to its allowed maximum power, according to the following relation:

$$P_{\mathrm{FC}} = \frac{E_b C_{r_{CM}}}{\eta_{\mathrm{DC/DC}}} \tag{10}$$

where E_b is the battery nominal capacity (i.e. 60 kWh), $\eta_{\mathrm{DC/DC}} = 0.93$ is the DC/DC inverter efficiency, while $C_{r_{CM}}$ is a reference battery C-rate coefficient during the CM. In particular, the value of $C_{r_{CM}}$ is set to 1C (that is the maximum continuous battery charge C-rate, as already stated in Section 6 and shown in Table 8), thus leading to $P_{\mathrm{FC}} = 64.5$ kW, in order to maximize the available power to charge the battery while keeping a relatively high efficient mode of operation for the FC. The battery is then used only to compensate the request of power whenever this is higher than that available from the FC. Otherwise, the battery is recharged by the FC and, when activated, also by means of regenerative braking. The battery power P_b in CM is therefore computed as follows:

$$P_b = P_{tot} - \eta_{\mathrm{DC/DC}} P_{\mathrm{FC}} \tag{11}$$

where negative values of P_b correspond to battery charging. In order to preserve and extend the battery life, the recharging current cannot exceed the maximum value allowed by the battery pack. Therefore, to avoid damaging of battery while recovering as much energy as possible, P_b is limited to a maximum value, that is 90 kW (i.e. the value corresponding to a C-rate equal to 1.5C, Table 8), during charging. Thus, in case that such a limit is reached during a regenerative braking event in CM, the FC output power is decreased according to the following equation:

$$P_{\mathrm{FC}} = \frac{P_{tot} + E_b C_{r_{CM_b}}}{\eta_{\mathrm{DC/DC}}} \tag{12}$$

with $C_{r_{CM_b}}$ being exactly 1.5C. Clearly, a negative value for P_{FC} from Eq. (12) is not allowed. Therefore, in this case, the FC is switched off (i.e. $P_{\mathrm{FC}} = 0$). The CM ends as the upper SoC threshold of 40% is reached and the hereafter referred to as Discharging Mode (DM) begins.
3. During the DM, the FC works to power the EM and to partially recharge the battery, which instead has a primary role to provide power for traction. Therefore, the FC power setpoint is reduced with respect to the CM mode, thus allowing for a higher efficiency operation. Specifically, in DM the FC power is set to the value corresponding to the maximum efficiency operating condition (η_{FC}=57%), which falls between 10 kW and 20 kW (Ballard Power Systems, private communication). As said, during this mode of operation, the battery can be still charged, mainly in regenerative mode but also if the instantaneous power request is lower than the FC power setpoint. Also, the same power limit as for CM is applied to the battery when recovering braking energy. Thus, the routine described by Eqs. 11,12 still holds, and it is used to compute and update the battery power and the FC power depending on the power demand. In DM, the battery discharges until its SoC reaches the lower threshold of 30%. From this moment on, the powertrain works so as to reproduce a CS mode of operation, by switching continuously from CM to DM and viceversa, to keep the battery SoC within the predefined range, until the hydrogen fuel stored on board is fully depleted.
4. Finally, once all the hydrogen is consumed, the CD mode of operation is reactivated, in order to lead the battery SoC to its lower limit (i.e. 30%) and exploit all the stored energy capacity.

By this energy management strategy, the FC is allowed to operate quite efficiently during the overall driving cycle, with mean power close to the mean power demand, as it will be shown in the next Section 8. In fact, since the FC operation does not directly depend from the requested

power at vehicle wheels, this approach allows its downsizing, which also leads to a reduction of costs related to the power unit architecture [48].

8. Simulation results

The control algorithm described in Section 7 has been implemented into a numerical model in MATLAB environment. Thus, the HEV behavior was simulated in order to evaluate the hydrogen fuel consumption, to check for assumptions consistency and verify the proposed design of the powertrain.

The initial battery SoC is assumed to be equal to 90% and a target driving range of 6 h is set. Since the reference driving cycles encompass only 600 s (Roll-on) and 540 s (Roll-off) of operation (Figs. 5 and 6), the target driving cycles are composed of a number of 36 and 40 consecutive reference driving cycles, for Roll-on and Roll-off, respectively. The time-step Δt for the numerical simulation is 0.25 s, which is equal to the sampling time of data from the ECU. The instantaneous hydrogen consumption is calculated, at each time-step, as follows:

$$c_{H_2} = \frac{P_{FC}\Delta t}{\eta_{FC} LHV_{H_2}} \tag{13}$$

where $LHV_{H_2} = 120$ MJ/kg is the lower heating value of hydrogen, and η_{FC} is the FC efficiency.

First, the all-electric range (AER), that is, the driving range of the vehicle in CD mode, and the amount of hydrogen fuel required to accomplish the target time of operation were evaluated. As a result, the AER of the HEV is equal to 1.0 h and 1.7 h for Roll-on and Roll-off operations, while the hydrogen consumption is equal to 11.5 kg and 5.9 kg in the two cases, respectively. Thus, by considering the most critical scenario, a hydrogen storage tank with approximately 12 kg of capacity can be selected, which would correspond to a storage volume of roughly 500 liters, if the hydrogen is assumed to be stored on-board at 350 bars in gaseous form.

The evaluation of the tank-to-wheel energy consumption considers both the electrical energy consumed by the batteries and the primary energy from fuel. Under a complete mission of 6 h, the former accounts for 36 kWh_e for both the YT operations, while the latter is equal to 383 kWh_f and 197 kWh_f, for Roll-on and Roll-off, respectively. This leads to an overall energy consumption of 419 kWh and 233 kWh for the two operations, which is significantly lower than the value estimated for the original Diesel–fueled vehicle: by considering a lower heating value for the Diesel of 44 MJ/kg and its consumption over the 6 h of continuous operation, estimated on the base of the acquired data, the primary energy for the Diesel–fueled vehicle amounts to 724 kWh_f and 538 kWh_f for Roll-on and Roll-off operations, respectively. Table 9 summarizes the results from this analysis. Once the hydrogen tank has been sized, the maximum driving range achievable by the HEV for either the considered YT port operations is computed. To this aim, also the availability of electrical energy stored on-board into the batteries, once the hydrogen storage system is emptied, should be considered. Therefore, a simulation was run until either the hydrogen fuel is fully depleted and no electrical energy for vehicle traction is available on-board (i.e. the battery SoC reaches its allowed lower limit, that is 30 %). The resulting driving ranges, in terms of hours of operation and traveled distances are reported in Table 10. Fig. 16 shows the obtained battery SoC profiles as a function of time, for the two YT operations. These are computed by considering that the SoC variation in time, $\dot{SoC}$, is defined by the following equations:

$$\begin{cases} \dot{SoC} = -\dfrac{P_b \eta_{b_c}}{E_b}, & \text{for charging} \quad (P_b < 0) \\ \dot{SoC} = -\dfrac{P_b}{\eta_{b_d} E_b}, & \text{for discharging} \quad (P_b \geqslant 0) \end{cases} \tag{14}$$

where η_{b_c} and η_{b_d} are the battery charging and discharging efficiencies, both set equal to 0.97, in line with typical values for the considered battery technology. The designed powertrain is able to satisfy the peak power requested by the selected driving cycles and to provide enough energy to accomplish the target driving ranges in a quite efficient way. This is particularly true for the Roll-off operation, for which the achievable driving range is almost the double of the target one. Despite being a non-optimized energy management strategy, the one applied leads to satisfactory results. From the battery SoC trajectory is noted indeed that the CD/CS mode of operation is well developed, with the battery SoC properly varying between the two imposed threshold limits during the CS phase. Also, the designed powertrain takes advantage from a quite efficient use of the FC. The CM and DM in Roll-on operation last for about 0.25 h each, thus leading to an average efficiency for the FC of 51 %. In Roll-off operation instead, the DM, during which the FC operates at the lowest power output with the highest efficiency is significantly more extended than the CM where, in contrast, the FC power output is higher and the efficiency lies to a lower value. In particular, in this case the batteries take roughly 0.16 h to get recharged from the lower to the higher threshold SoC in CM, while their discharge in CS lasts for about 0.74 h. This behavior leads to an average efficiency for the FC of 53 %. Figs. 17 and 18 show the power profiles, normalized to the maximum requested power ($P_{tot_{max}}$), for battery and FC during consecutive CM and DM stages of Roll-on operation, respectively, along with the vehicle speed profile. The trends depicted in Figs. 17 and 18 refer to a specific interval of time during the CS mode operation, that is between 3.05 h and 3.55 h from the start, and they are meant to be illustrative examples. The FC power output results to be almost constant during both the CM and DM phases, and equal to its set value, respectively. The slight deviations from its two designed points of operation are due to the occurring of regenerative braking events, which decrease the power demand at the FC, with clear advantages in terms of its efficiency. Similar trends are obtained for the case of Roll-off operation. The computed FC mean power, during the whole driving cycle, are equal to 39.7 kW and 23.5 kW for Roll-on and Roll-off operations, respectively. These values are close to the mean power requested by the HEV during the considered port operations (i.e. 34.0 kW and 20.9 kW for Roll-on and Roll-off, respectively). This further confirms the suitability of the FC stack choice, for the designed powertrain.

Also, the battery power profiles for both the YT operations are consistent with those for the overall power demand, as expected. In the most demanding scenario, that is the Roll-on operation, the battery power output hits a peak of 176.3 kW during the initial CD mode of operation and a peak of 162.8 kW during the DM in CS mode of operation. In particular, the battery maximum discharge C-rate, which occurs during the CD, results to be equal to 2.9C. This value is reached only in a very narrow interval of time, corresponding to a peak power request

Table 9
Tank-to-wheel analysis: comparison between the hybrid electric YT and the Diesel–fueled YT on-board fuel and energy requirements to accomplish the target RoRo port operations.

	hybrid electric YT			Diesel-fueled YT	
	electric energy [kWh_e]	c_{H_2} [kg]	primary energy [kWh_f]	c_{Diesel} [kg]	primary energy [kWh_f]
Roll-on	36	11.5	383	59.2	724
Roll-off	36	5.9	197	44.0	538

Table 10
Driving ranges for Roll-on and Roll-off port operations.

	time of operation [h]	traveled distance [km]
Roll-on	6.2	57.0
Roll-off	10.7	97.5

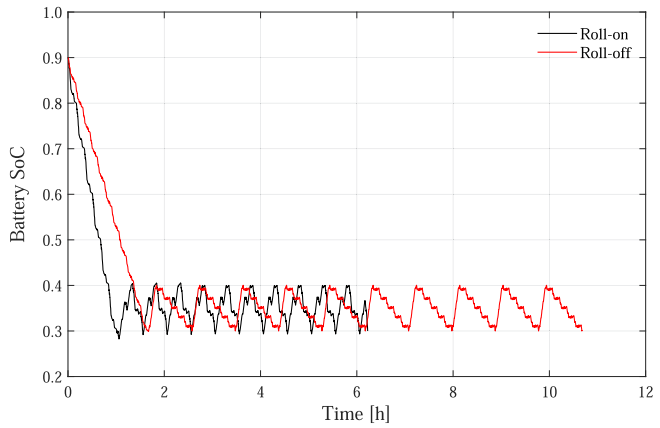

Fig. 16. Battery SoC as a function of time, for the YT Roll-on and Roll-off operations.

when the loaded vehicle climbs the first slope. Moreover, it is lower than the allowed maximum (i.e. 5C), thus it can be considered acceptable.

To conclude, the presented results provide evidences that such a preliminary design of a fuel cell/battery hybrid powertrain for the considered heavy-duty vehicle is promising and could open the path toward the development of an innovative and efficient propulsion system. The findings from this work provide indeed useful indications for further optimization, both in terms of powertrain architecture and components design, as well as from an energy management standpoint.

9. Conclusions

In this work, the preliminary design of a fuel cell/battery hybrid powertrain for a yard truck used in port logistics has been proposed on the base of real driving conditions, and an exhaustive analysis of its energy performance has been conducted in order to assess the capability of the hybrid vehicle to accomplish the target port operations. The results are promising: the proposed hybrid electric vehicle outperforms the original Diesel vehicle, in terms of power and energy requirements, while producing zero local emissions. The efficient use of the FC allows a

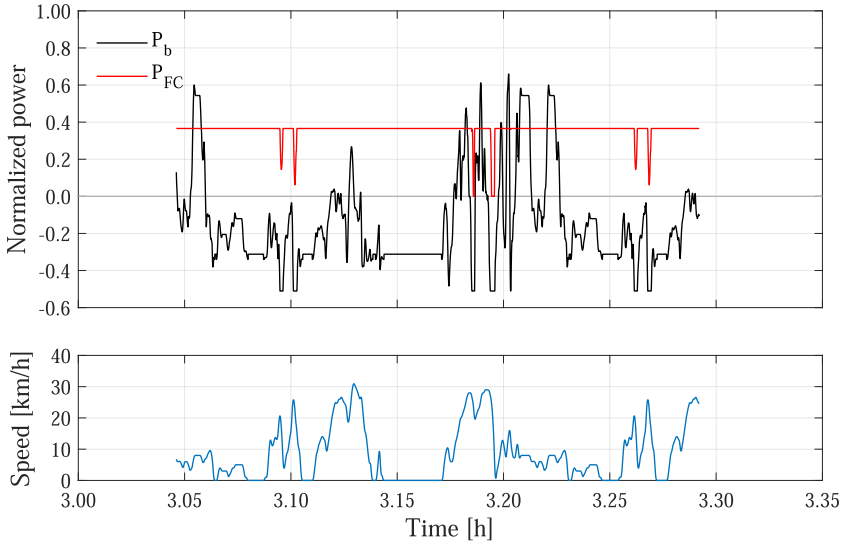

Fig. 17. Top: battery and FC power demands during CM in Roll-on operation. Bottom: vehicle speed profile.

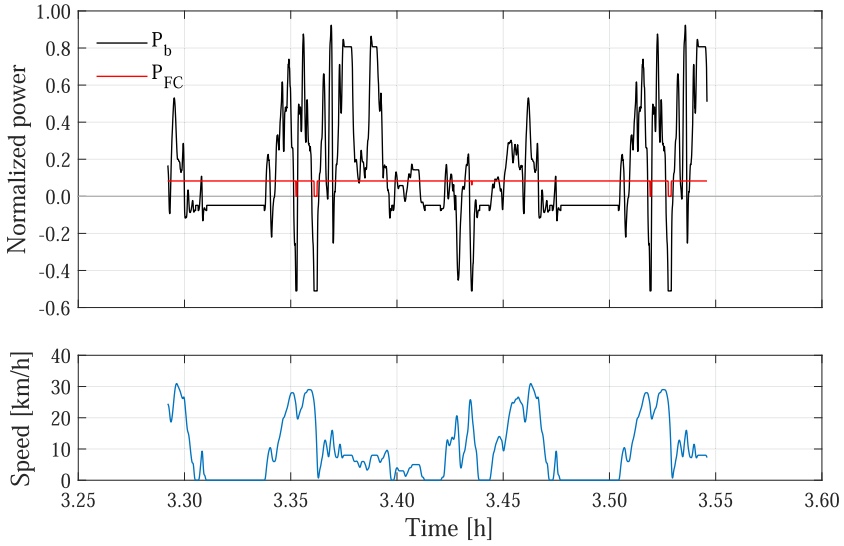

Fig. 18. Top: battery and FC power demands during DM in Roll-on operation. Bottom: vehicle speed profile.

relatively low consumption of hydrogen.

To the authors' knowledge, this is a first-of-a-kind analysis, as none of all previous known works related to hybrid electric powertrain implementations are focused on port applications. The study also provides driving and duty cycles for real RoRo operations, which may be used as standard references in future researches.

This work paves the way for the development of an innovative FC industrial vehicle for applications in port terminals, thus promoting the decarbonisation of the port logistic industry by implementing hydrogen technologies already adopted in other sectors. Future works will be devoted to the implementation of an optimal energy management strategy, with the aim of achieving minimization of the hydrogen consumption over the target port operation. Also, multiple mission profiles will be identified, in order to test the designed HEV powertrain configuration and provide an applicable, flexible and efficient solution for a wide range of operations.

CRediT authorship contribution statement

G.Di Ilio: Conceptualization, Methodology, Investigation, Writing - original draft. **P.Di Giorgio:** Conceptualization, Methodology, Software. **L. Tribioli:** Investigation, Writing - review & editing. **G. Bella:** Supervision. **E. Jannelli:** Conceptualization, Writing - review & editing, Supervision, Funding acquisition.

Declaration of Competing Interest

The authors declare that they have no known competing financial interests or personal relationships that could have appeared to influence the work reported in this paper.

Acknowledgements

This research has received funding from the Fuel Cells and Hydrogen 2 Joint Undertaking (JU) under grant agreement No 826339, project H2Ports - Implementing Fuel Cells and Hydrogen Technologies in Ports. The JU receives support from the European Union's Horizon 2020 research and innovation programme and Spain, Denmark, Netherlands, Italy. The authors gratefully acknowledge Grimaldi Euromed SpA for having allowed the measurement campaign at Grimaldi's Terminal in port of Salerno. The authors also gratefully acknowledge Ciro Santoru and all the Manuport (a Terberg Group Company) Operators who have contributed to the vehicle data acquisition.

References

[1] European Commission. Annual Report on CO2 Emissions from Maritime Transport, SWD2020 82; 2019.
[2] International Maritime Organization. Third IMO GHG Study; 2014.
[3] Dalsøren S, Eide M, Endresen Ø, Mjelde A, Gravir G, Isaksen I. Update on emissions and environmental impacts from the international fleet of ships: the contribution from major ship types and ports. Atmos Chem Phys 2009;9:2171–94. https://doi.org/10.5194/acp-9-2171-2009.
[4] European Commission. Entec UK Limited, Quantification of emissions from ships associated with ship movements between ports in the European Community; 2002.
[5] Merk O. Shipping emissions in ports. International Transport Forum, Discussion Paper N. 2014-20.
[6] Balcombe P, Brierley J, Lewis C, Skatvedt L, Speirs J, Hawkes A, Staffell I. How to decarbonise international shipping: Options for fuels, technologies and policies. Energy Convers Manag 2019;182:72–88. https://doi.org/10.1016/j.enconman.2018.12.080.
[7] Fernández A, Péez B, Trashorras A, Artime S, Fernández J, Caballín J. Optimization of the propulsion plant of a Liquefied Natural Gas transport ship. Energy Convers Manag 2020;224:113398. https://doi.org/10.1016/j.enconman.2020.113398.
[8] Burel F, Taccani R, Zuliani N. Improving sustainability of maritime transport through utilization of Liquefied Natural Gas (LNG) for propulsion. Energy 2013;57:412–20. https://doi.org/10.1016/j.energy.2013.05.002.
[9] Wang S, Notteboom T. The adoption of liquefied natural gas as a ship fuel: a systematic review of perspectives and challenges. Transp Rev 2014;34:749–74. https://doi.org/10.1080/01441647.2014.981884.
[10] Giap V, Lee Y, Kim Y, Ahn K, Kim D, Lee J. System simulation and exergetic evaluation of hybrid propulsion system for crude oil tanker: a hybrid of solid-oxide fuel cell and gas engine. Energy Convers Manag 2020;223:113265. https://doi.org/10.1016/j.enconman.2020.113265.
[11] Al-Falahi M, Nimma K, Jayasinghe S, Enshaei H, Guerrero J. Power management optimization of hybrid power systems in electric ferries. Energy Convers Manag 2018;172:50–66. https://doi.org/10.1016/j.enconman.2018.07.012.
[12] Biert LV, Godjevac M, Visser K, Aravind P. A review of fuel cell systems for maritime applications. J Power Sources 2016;327:345–64. https://doi.org/10.1016/j.jpowsour.2016.07.007.
[13] De-Troya J, Álvarez C, Garrido C, Carral L. Analysing the possibilities of using fuel cells in ships. Int J Hydrogen Energy 2016;41:2853–66. https://doi.org/10.1016/j.ijhydene.2015.11.145.
[14] Lion S, Vlaskos I, Taccani R. A review of emissions reduction technologies for low and medium speed marine Diesel engines and their potential for waste heat recovery. Energy Convers Manag 2020;207:112553. https://doi.org/10.1016/j.enconman.2020.112553.
[15] Ballini F, Bozzo R. Air pollution from ships in ports: the socio-economic benefit of cold-ironing technology. Res Transp Bus Manag 2015;17:92–8. https://doi.org/10.1016/j.rtbm.2015.10.007.
[16] Sdoukopoulos E, Boile M, Tromaras A, Anastasiadis N. Energy efficiency in European ports: state-of-practice and insights on the way forward. Sustainability 2019;11:4952. https://doi.org/10.3390/su11184952.
[17] Acciaro M, Ghiara H, Cusano M. Energy management in seaports: a new role for port authorities. Energy Policy 2014;71:4–12. https://doi.org/10.1016/j.enpol.2014.04.013.
[18] Iris C, Lam J. A review of energy efficiency in ports: operational strategies, technologies and energy management systems. Renew Sustain Energy Rev 2019;112:170–82. https://doi.org/10.1016/j.rser.2019.04.069.
[19] Rizzoni G, Ahmed Q, Arasu M, Oruganti PS. Transformational technologies reshaping transportation-an academia perspective [Tech. rep.]. SAE Technical Paper; 2019. doi:10.4271/2019-01-2620.
[20] Hwang J. Sustainability study of hydrogen pathways for fuel cell vehicle applications. Renew Sustain Energy Rev 2013;19:220–9. https://doi.org/10.1016/j.rser.2012.11.033.
[21] Colella W, Jacobson M, Golden D. Switching to a U.S. hydrogen fuel cell vehicle fleet: the resultant change in emissions, energy use, and greenhouse gases. J Power Sources 2005;150:150–81. https://doi.org/10.1016/j.jpowsour.2005.05.092.
[22] Tang Y, Yuan W, Pan M, Wan Z. Experimental investigation on the dynamic performance of a hybrid PEM fuel cell/battery system for lightweight electric vehicle application. Appl Energy 2011;88:68–76. https://doi.org/10.1016/j.apenergy.2010.07.033.
[23] Di Trolio P, Di Giorgio P, Genovese M, Frasci E, Minutillo M. A hybrid power-unit based on a passive fuel cell/battery system for lightweight vehicles. Appl Energy 2020;279:115734. https://doi.org/10.1016/j.apenergy.2020.115734.
[24] Kast J, Vijayagopal R, Gangloff J, Marcinkoski J. Clean commercial transportation: medium and heavy duty fuel cell electric trucks. Int J Hydrogen Energy 2017;42:4508–17. https://doi.org/10.1016/j.ijhydene.2016.12.129.
[25] Di Giorgio P, Di Trolio P, Jannelli E, Minutillo M, Conte FV. Model based preliminary design and optimization of internal combustion engine and fuel cell hybrid electric vehicle. Energy Proc 2018;148:1191–1198. aTI 2018–73rd Conference of the Italian Thermal Machines Engineering Association. doi:10.1016/j.egypro.2018.08.022.
[26] Ferrara A, Jakubek S, Hametner C. Energy management of heavy-duty fuel cell vehicles in real-world driving scenarios: robust design of strategies to maximize the hydrogen economy and system lifetime. Energy Convers Manag 2021;232:113795. https://doi.org/10.1016/j.enconman.2020.113795.
[27] Barelli L, Bidini G, Ciupageanu DA, Pianese C, Polverino P, Sorrentino M. Stochastic power management approach for a hybrid solid oxide fuel cell/battery auxiliary power unit for heavy duty vehicle applications. Energy Convers Manag 2020;221:113197. https://doi.org/10.1016/j.enconman.2020.113197.
[28] Samsun R, Krupp C, Baltzer S, Gnorich B, Peters R, Stolten D. A battery-fuel cell hybrid auxiliary power unit for trucks: analysis of direct and indirect hybrid configurations. Energy Convers Manag 2016;127:312–23. https://doi.org/10.1016/j.enconman.2016.09.025.
[29] Ribau J, Silva C, Sousa J. Efficiency, cost and life cycle CO2 optimization of fuel cell hybrid and plug-in hybrid urban buses. Appl Energy 2014;129:320–35. https://doi.org/10.1016/j.apenergy.2014.05.015.
[30] Villani M, Lombardi S, Tribioli L. Performance evaluation of a heavy-duty diesel truck retrofitted with waste heat recovery and hybrid electric systems. SAE Int J Electrified Vehicles 2020;9(14-09-01-0004):41–59. https://doi.org/10.4271/08-09-01-0004.
[31] Lu X, Wang P, Meng L, Chen C. Energy optimization of logistics transport vehicle driven by fuel cell hybrid power system. Int J Hydrogen Energy 2019;199:111887. https://doi.org/10.1016/j.enconman.2019.111887.
[32] Hosseinzadeh E, Rokni M, Advani S, Prasad AK. Performance simulation and analysis of a fuel cell/battery hybrid forklift truck. Int J Hydrogen Energy 2013;38:4241–9. https://doi.org/10.1016/j.ijhydene.2013.01.168.
[33] Terberg Manual.www.terbergbenschop.nl (accessed March 1, 2021), Terberg Benschop B.V.
[34] Ehsani M, Gao Y, Gay S, Emadi A. Modern electric, hybrid electric, and fuel cell vehicles: fundamentals, theory, and design. CRC Press; 2009.
[35] Wong J. Theory of ground vehicles. John Wiley & Sons; 2008.
[36] Filippo GD, Marano V, Sioshansi R. Simulation of an electric transportation system at The Ohio State University. Appl Energy 2014;113:1686–91. https://doi.org/10.1016/j.apenergy.2013.09.011.
[37] Lombardi S, Tribioli L, Guandalini G, Iora P. Energy performance and well-to-wheel analysis of different powertrain solutions for freight transportation. Int J

Hydrogen Energy 2020;45:12535–54. https://doi.org/10.1016/j.ijhydene.2020.02.181.
[38] Danfoss EM-PMI375-T1100 Data Sheet.www.danfoss.com (accessed March 1, 2021), Danfoss.
[39] Satyavani T, Srinivas Kumar A, Subba Rao P. Methods of synthesis and performance improvement of lithium iron phosphate for high rate li-ion batteries: a review. Eng Sci Technol 2016;19(1):178–88. https://doi.org/10.1016/j.jestch.2015.06.002.
[40] Ballard FCmove-HD Data Sheet.www.ballard.com (accessed March 1, 2021), Ballard Power Systems.
[41] Sciarretta A, Guzzella L. Control of hybrid electric vehicles. IEEE Control Syst Mag 2007;27(2):60–70. https://doi.org/10.1109/MCS.2007.338280.
[42] Serrao L, Onori S, Rizzoni G. A comparative analysis of energy management strategies for hybrid electric vehicles. J Dyn Syst Meas Control 133(3). doi:doi.org/10.1115/1.4003267.
[43] Onori S, Tribioli L. Adaptive pontryagin's minimum principle supervisory controller design for the plug-in hybrid gm chevrolet volt. Appl Energy 2015;147:224–34. https://doi.org/10.1016/j.apenergy.2015.01.021.
[44] Tribioli L, Cozzolino R, Chiappini D, Iora P. Energy management of a plug-in fuel cell/battery hybrid vehicle with on-board fuel processing. Appl Energy 2016;184:140–54. https://doi.org/10.1016/j.apenergy.2016.10.015.
[45] Geng B, Mills J, Sun D. Two-stage energy management control of fuel cell plug-in hybrid electric vehicles considering fuel cell longevity. IEEE Trans Veh Technol 2012;61:498–508. https://doi.org/10.1109/TVT.2011.2177483.
[46] Wu J, Zhang N, Tan D, Chang J, Shi W. A robust online energy management strategy for fuel cell/battery hybrid electric vehicles. Int J Hydrogen Energy 2020;45(27):14093–107. https://doi.org/10.1016/j.ijhydene.2020.03.091. URL: https://www.sciencedirect.com/science/article/pii/S0360319920310284.
[47] Wang Y, Advani SG, Prasad AK. A comparison of rule-based and model predictive controller-based power management strategies for fuel cell/battery hybrid vehicles considering degradation. International Journal of Hydrogen Energy 2020;45(58):33948–56. https://doi.org/10.1016/j.ijhydene.2020.09.030.
[48] Dell R, Moseley P, Rand D. Towards sustainable road transport. Academic Press; 2014.